Journal of
Materials Chemistry B

PAPER

View Article Online
View Journal

Published on 24 August 2015. Downloaded by Universitat de Barcelona on 04/09/2015 11:30:50.

Cite this: DOI: 10.1039/c5tb01345c

Multifunctionalized polyurethane–polyurea nanoparticles: hydrophobically driven self-stratification at the o/w interface modulates encapsulation stability†

Pau Rocas,*[a] Yolanda Fernández,[b] Simó Schwartz Jr,[b] Ibane Abasolo,[b] Josep Rocas*[c] and Fernando Albericio*[def]

Received 7th July 2015,
Accepted 24th August 2015

DOI: 10.1039/c5tb01345c

www.rsc.org/MaterialsB

Polyurethane–polyurea (PUUa) reactive prepolymers with adjusted hydrophobic and hydrophilic dangling chains to achieve multiwalled sub-30 nm nanoparticles are presented. The combination of an amphiphilic and a hydrophobic prepolymer at the oil–water interface creates a stratified shell by hydrophobic interactions. These novel nanostructures enhance the encapsulation stability of lipophilic compounds compared to monowalled nanostructures and facilitate the selective and ordered functionalization along the multiwalled shell with bioactive motifs. As proof of concept, PUUa nanoparticles have been engineered with disulfide bonds and an $\alpha_v\beta_3$ integrin-selective cyclic RGD peptide (cRGDfK) providing our system with glutathione (GSH) triggered controlled release and cell targeting specificity to U87 tumor cells.

1. Introduction

Merging cross-functional fields such as chemistry, engineering, medicine, and biology to achieve multifunctional stimuli responsive drug delivery systems (DDSs) is one of the major challenges in modern medicine.[1,2] Therefore, large efforts are being undertaken to unravel the unknowns which means that even today an *in vivo* reliable and efficient smart nano-system has not been completely achieved. Obviously, in the past decade, great progress has been made in the creation of advanced DDSs, although, these are usually formed through the emulsification of a hydrophobic drug in water using external surfactants.[3,4] However, this kind of DDS commonly lacks chemical tailorability, encapsulation efficiency, targeting selectivity, biocompatibility and controlled degradability, among others. One recurrent issue in top used multiblock polymeric systems like PLA, PLGA, PMMA, *etc.* is the lack of reactive sites that enable multifunctionality. So, smarter nano-systems with complex structures such as dendrimers or multibranched polymers arose. Sadly, sometimes the difficult syntheses and costly purification steps limit their industrial and commercial translation. Accordingly, nanoparticles (NPs) fulfilling these structural, delivery and biological requirements are needed in the demanding field of nanomedicine. The scientific community is nowadays highly concerned with the possibility of achieving not only multifunctionality but also self-assembled nanostructured architectures for multiple purposes.[5,6] It has been proven that, the capacity of polymers to be self-structured, forming the shell of a nano-system is directly related to the ease with which their molecular structure can be modified. So, the tailored design of a polymer is only viable when it is not only chemically tunable but also cost-efficient.[7,8] Thus, to get structural control at the nano-level, a different kind of prepolymer with adjustable physico-chemical and bioactive characteristics is needed. Therefore, polyurethanes and polyureas are potential choices to fulfill such needs. In this regard, very few publications have reported the application of reactive polymeric surfactants containing free isocyanate groups.[9–11] The high reactivity of isocyanates with hydroxyl and/or amine containing precursors allows fast structure stabilization by crosslinking and the efficient functionalization of micro and nanoparticles *via* polyurethane and/or polyurea bonds. Specifically, PUUa diisocyanate prepolymers can create stable shells by anchoring a wide range of nucleophile-containing (amines, thiols, alcohols, *etc.*) bioactives.[12] For example, polyisocyanates with high functionality ($f > 2$) allow the multiple

[a] *Institute for Research in Biomedicine (IRB Barcelona), Baldiri Reixac 10, 08028 Barcelona, Spain. E-mail: pau.rocas@irbbarcelona.org*
[b] *CIBBIM-Nanomedicine, VHIR Vall d'Hebron Institut de Recerca, 08035 Barcelona, Spain*
[c] *Nanobiotechnological Polymers Division, Ecopol Tech S.L., Indústria 7, 43720 L'Arboç, Tarragona, Spain. E-mail: direccio@ecopoltech.com*
[d] *Department of Organic Chemistry, University of Barcelona, Martí Franquès 1-11, 08028 Barcelona, Spain. E-mail: albericio@ub.edu*
[e] *School of Chemistry & Physics, University of Kwazulu-Natal, 4041 Durban, South Africa*
[f] *CIBER-BBN, Networking Centre on Bioengineering Biomaterials and Nanomedicine, 08028 Barcelona, Spain*

† Electronic supplementary information (ESI) available. See DOI: 10.1039/c5tb01345c

Published on 24 August 2015. Downloaded by Universitat de Barcelona on 04/09/2015 11:30:50.

bonding of bioactive molecules that provides targeting properties and at the same time enables modulation of their intrinsic hydrophilic–lipophilic balance.[13,14] It should be noted that to ensure the good biocompatibility and reduced toxicity of biodegraded products aliphatic isocyanates need to be selected instead of aromatic ones.[15–17] Since the late sixties their biocompatibility for biomedical use has been well proven as it is one of the materials of choice in clinical use for the development of catheters, stents, valves, *etc.* The quantitative synthetic procedures, facile scalable processes and broad chemistry of PUUa open up an infinite range of potential functionalities that can be incorporated. Multiple chemical complexities, biodegradation, targeting and biocompatibility are some of the clear advantages that PUUa polymers can bring to the table as future smart and nanostructured DDSs.

Herein we depict the combination of two PUUa prepolymers (one amphiphilic and the other hydrophobic) in aqueous media to create hydrophobically ordered shells. The novel prepolymers contain dangling chains of sharply different polarities to promote controlled stratification at the oil–water interface to achieve multiwalled nanostructures and bear terminal isocyanate groups for a final crosslinking step to ''freeze'' the preformed architecture. These nanostructures are designed to improve the encapsulation stability of hydrophobic cargo, providing deeper encapsulation in the NP core compared to monowalled nanostructures where the cargo is closer to the shell surface and released in bursts under *in vivo* conditions.[18]

2. Materials and methods

2.1. Chemicals

Cyclo(-Arg-Gly-Asp-D-Phe-Lys) (cRGDfK) was synthesized in house according to previously reported protocols.[19] YMER N-120 was kindly provided by Perstorp (Perstorp, Sweden) and *N*-Coco-1,3-propylenediamine (Genamin TAP 100D) by Clariant (Barcelona, Spain). A capric/caprylic triglyceride mixture (Crodamol GTCC) was obtained from Croda (Barcelona, Spain) and Bayhydur 3100 was purchased from Bayer (Leverkusen, Germany). If not indicated otherwise, all other reagents were purchased from Sigma-Aldrich (St. Louis, MO, USA). Extra dry acetone was used during all of the synthetsis processes.

2.2. Cell lines and cell culture

Human glioblastoma cell line (U87-MG) and human colorectal cancer cell line (HT-29) used in cell internalization assays and human cervix carcinoma cell line (HeLa) used in cytotoxicity assays were obtained from the American Type Culture Collection. All cell lines were maintained as recommended. Briefly, U87-MG cells were maintained in DMEM medium and HT-29 and HeLa cells in RPMI 1640 medium, both from Life Technologies. All media were supplemented with 10% heat-inactivated fetal bovine serum (FBS) (56 °C, 30 min), penicillin (100 U mL^{-1}), streptomycin (100 μg mL^{-1}) and Fungizone (250 ng mL^{-1}) (Life Technologies, Madrid, Spain). Cells were maintained under a humid atmosphere at 37 °C with 5% CO_2.

2.3. Experimental methods

2.3.1. Synthesis of reactive prepolymers for multiwalled PUUa NP preparation

2.3.1.1. Preparation of the reactive amphiphilic prepolymer (Amphil). To synthesize the amphiphilic prepolymer, a 500 mL four-necked reaction vessel was pre-heated at 50 °C and purged with nitrogen. Then, YMER N-120 (5.50 g, 5.5 mmol), 2-hydroxyethyl disulfide (DEDS) (0.15 g, 1 mmol), Crodamol GTCC (0.75 g) and IPDI (3.38 g, 15 mmol) were added to the reaction vessel under mechanical stirring with dibutyltin dilaurate (DBTL) as catalyst (3 mg, 4.65 μmol). The polyaddition reaction was maintained under these conditions until DEDS and YMER reacted quantitatively with IPDI as followed using FT-IR (Fig. S5, ESI†) and automatic titration[20] (Fig. S2, ESI†). At this point, the vessel was cooled to 40 °C and Genamin TAP 100D (1.45 g, 4.44 mmol) dissolved in 10 g of acetone was added under constant stirring and left to react for 30 min (Fig. S1, ESI†). The formation of polyurethane and polyurethane–polyurea prepolymers was followed by automatic titration (Fig. S2, ESI†) and FT-IR (Fig. S5, ESI†) and characterized by NMR[21] (Fig. S7, ESI†).

2.3.1.2. Preparation of the reactive hydrophobic prepolymer (Hyfob). To synthesize the hydrophobic prepolymer, a Schlenk flask of 20 mL was pre-heated at 50 °C and purged with nitrogen. Then, DEDS (0.15 g, 1 mmol) and IPDI (0.485 g, 2.18 mmol) in acetone (7 g) were added with DBTL as catalyst (0.24 mg, 0.37 μmol) and left to react for 1 h with magnetic stirring. At this point, the Schlenk flask was cooled to 40 °C and Genamin TAP 100D (0.15 g, 0.5 mmol) dissolved in 3 g of acetone was added under constant stirring and left to react for 30 min (Fig. S1, ESI†). The formation of polyurethane and polyurethane–polyurea prepolymers was followed using FT-IR (Fig. S4, ESI†) and they were characterized using NMR[21] (Fig. S7, ESI†).

2.3.1.3. Preparation of the Bayhydur 3100–cRGDfK conjugate (B3100–cRGDfK). The peptide cRGDfK (36 mg, 0.0596 mmol) was dissolved in phosphate buffered saline (PBS) (1 mL, 5 °C) and 10 μL of pure triethylamine were added to the mixture (pH 10). Then, the previous solution was mixed with Bayhydur 3100 linker (B3100) (125 mg, 0.167 mmol) and allowed to react for 2 h at 5 °C under constant stirring (Fig. S1, ESI†). The bonding of one cRGDfK molecule per B3100 linker, the reaction kinetics between cRGDfK and B3100, and the total concentration of linked cRGDfK in PUUa NP–RGD was followed using MALDI-TOF MS (Fig. S9, ESI†) and HPLC (Fig. S10 and Table S1, ESI†).

2.3.2. Synthesis of the multiwalled polyurethane–polyurea nanoparticles

2.3.2.1. PUUa NPs synthesis. A previously homogenized aliquot of Amphil + Hyfob (1.69 g, mass ratio Amphil 13.35 : 1 Hyfob) (see Section 2.3.1) was added in a round-bottom flask containing B3100 (125 mg, 0.167 mmol) under a nitrogen atmosphere. This organic mixture was then emulsified in PBS (16 mL, pH 7.4, 5 °C) with a magnetic stirrer in an ice bath to prevent isocyanate reacting with water. Once emulsified, L-lysine was added (68.56 mg, 0.47 mmol) and the interfacial polyaddition reaction was

This journal is © The Royal Society of Chemistry 2015

Published on 24 August 2015. Downloaded by Universitat de Barcelona on 04/09/2015 11:30:50.

followed using FT-IR. After 30 min, DETA (32.18 mg, 0.31 mmol) was added and the crosslinked nanoparticles were formed by a second interfacial polyaddition as proven by FT-IR. Acetone was mildly removed in a rotavapor. PUUa NPs were dialysed (100 000 MWCO, Spectrum Laboratories, California, USA) against pure water for 72 h for zeta potential experiments. For *in vitro* experiments PUUa NPs were dialysed against PBS for 72 hours.

2.3.2.2. PUUa DiI loaded NPs synthesis (PUUa NP-DiI). These NPs were synthesized as previously described (see Section 2.3.2.1) by adding Amphil + Hyfob in a round bottom flask containing DiI (2.5 mg, 2.67 μmol) as a fluorophore. The organic mixture was homogenized and subsequently, Section 2.3.2.1 was followed without modification.

2.3.2.3. PUUa DiO loaded NPs synthesis (PUUa NP-DiO). These NPs were synthesized as previously described (see Section 2.3.2.2) using DiO (2.5 mg, 2.83 μmol) as the fluorophore instead of DiI.

2.3.2.4. All-in-one PUUa NP formation (PUUa NP-DiI–RGD). These PUUa NPs were synthesized as previously described (see Section 2.3.2.1) using B3100–cRGDfK as a targeting conjugate. The Amphil + Hyfob organic mixture was mixed with the previously described B3100–cRGDfK conjugate solution (see Section 2.3.1.3) (16% w/w) followed by emulsification in PBS (16 mL, pH 7.4, 5 °C) with a magnetic stirrer in an ice bath to prevent isocyanate reacting with water. At this point, Section 2.2.1 was followed without modification.

2.3.2.5. PUUa NPs DETA crosslinked. Section 2.3.2.1 was followed but crosslinked by interfacial polyaddition only with DETA (64.36 mg, 0.62 mmol).

2.3.2.6. PUUa NPs Lys crosslinked. Section 2.3.2.1 was followed but crosslinked by interfacial polyaddition only with L-lysine (137.12 mg, 0.94 mmol).

2.3.3. Synthesis of the reactive prepolymer for monowalled PUUa NP preparation

2.3.3.1. Preparation of the reactive amphiphilic prepolymer (Amphil). To allow a logical comparison between nanoparticles, the monowalled ones contained the same total amount of monomer as the multiwalled ones but just in one Amphil prepolymer. To synthesize the amphiphilic prepolymer, a 500 mL four-necked reaction vessel was pre-heated at 50 °C and purged with nitrogen. Then, YMER N-120 (5.50 g, 5.5 mmol), 2-hydroxyethyl disulfide (DEDS) (0.30 g, 2 mmol), Crodamol GTCC (0.75 g) and IPDI (3.866 g, 17 mmol) were added to the reaction vessel under mechanical stirring with dibutyltin dilaurate (DBTL) as catalyst (3.24 mg, 5.02 μmol). The polyaddition reaction was maintained under these conditions until DEDS and YMER reacted quantitatively with IPDI as followed using FT-IR and automatic titration.[20] At this point, the vessel was cooled to 40 °C and Genamin TAP 100D (1.6 g, 4.94 mmol) dissolved in 10 g of acetone was added under constant stirring and left to react for 30 min. The formation of polyurethane and polyurethane–polyurea prepolymers was followed using FT-IR.

2.3.4. Synthesis of the monowalled polyurethane–polyurea nanoparticles

2.3.4.1. PUUa DiI loaded NPs synthesis (PUUa NP-DiI). A previously homogenized aliquot of Amphil (1.69 g) (see Section 2.3) was added in a round-bottom flask containing DiI (2.5 mg, 2.67 μmol) as a fluorophore and B3100 (125 mg, 0.167 mmol) under a nitrogen atmosphere. This organic mixture was then emulsified in PBS (16 mL, pH 7.4, 5 °C) with a magnetic stirrer in an ice bath to prevent isocyanate reacting with water. Once emulsified, L-lysine was added (68.56 mg, 0.47 mmol) and the interfacial polyaddition reaction was followed using FT-IR. After 30 min, DETA (32.18 mg, 0.31 mmol) was added and the crosslinked nanoparticles were formed by a second interfacial polyaddition as proven using FT-IR. Acetone was mildly removed in a rotavapor. PUUa NPs were dialysed (100 000 MWCO, Spectrum Laboratories, California, USA) against pure water for 72 h for FRET experiments.

2.3.4.2. PUUa DiO loaded NPs synthesis (PUUa NP-DiO). These NPs were synthesized as previously described (see Section 2.3.4.1) using DiO (2.5 mg, 2.83 μmol) as the fluorophore instead of DiI.

2.4. Analytical techniques

2.4.1. Transmission electron microscopy. The nanoparticle morphology was studied using a Jeol JEM 1010 (Peabody, MA, USA). A drop of 10 mg mL^{-1} nanoparticles in water was deposited on a 200 mesh copper grid coated with 0.75% FORMVAR for 1 min. Nanoparticle excess was removed by fresh milliQ water contact for 1 min. Then, a drop of uranyl acetate 2% w/w in water was deposited on the grid for 30 s. The uranyl acetate excess was blotted off and air-dried before measurement. For the degradation experiment, 10 μL of filtered (0.22 μm) PUUa NPs (100 mg mL^{-1}) were added into 1 mL of GSH (10 mM) solution and incubated at 37 °C for 24 h under constant stirring. For statistical analysis, 5 different zones of the copper grid were randomly counted with ImageJ software (NIH, Bethesda, MD, USA).

2.4.2. B3100–cRGDfK reaction control. The reaction solution containing B3100 and cRGDfK (see Section 2.1.3) was analysed at 0 and 2 hours of reaction. Analytical HPLC runs of B3100–cRGDfK were performed in a WATERS 2998 HPLC (Milford, MA, USA) using a X-Bridge BEH130, C18, 3.5 μm, 4.6 × 100 mm reverse phase column with the following gradient: 5–15% B in 9 min at a flow rate of 1 mL min^{-1}; eluent A: H_2O with 0.045% TFA (v/v); eluent B: CH_3CN with 0.036% TFA.

2.4.3. PUUa NP–RGD conjugation yield quantification. A calibration curve was obtained by preparing 5 standard solutions of the cRGDfK peptide containing L-phenylalanine amide as the internal standard for quantitative HPLC analysis. Analytical HPLC runs of the PUUa NP–RGD were performed in a WATERS 2998 HPLC (Milford, MA, USA) using a X-Bridge BEH130, C18, 3.5 μm, 4.6 × 100 mm reverse phase column with the following gradient: 5–30% B in 9 min at a flow rate of 1 mL min^{-1}; eluent A: H_2O with 0.045% TFA (v/v); eluent B: CH_3CN with 0.036% TFA.

Published on 24 August 2015. Downloaded by Universitat de Barcelona on 04/09/2015 11:30:50.

2.4.4. Size distribution by DLS. PUUa NPs and PUUa NP–RGD were analysed on a Malvern Zetasizer Nano-ZS90 (Malvern, UK) at 1 mg mL^{-1} in pure water at 37 °C.

2.4.5. Zeta potential measurements. PUUa NPs and PUUa NP–RGD were analysed on a Malvern Zetasizer Nano-ZS90 (Malvern, UK) at 20 mg mL^{-1} in pure water at 37 °C.

2.4.6. Infrared spectra. IR spectroscopy was performed using a FT-IR Nexus Termo Nicolet 760 (Waltham, MA, USA) by depositing a drop of the previously dissolved prepolymer at 1% in acetone on a NaCl or BaF_2 (for aqueous samples) disk.

2.4.7. Automatic titration. A prepolymer sample after being dissolved in dry toluene reacted with the excessive di-*n*-butylamine standard, and residual di-*n*-butylamine was back-titrated with 1 M hydrochloric acid up to the endpoint. The content of isocyanate was calculated from the titration volume.

2.4.8. FRET experiments

Control experiment. To evaluate the kinetics of hydrophobic molecule leakage, 10 μL of 100 mg mL^{-1} PUUa NPs containing DiI (0.15 mg mL^{-1}) and 10 μL of 100 mg mL^{-1} PUUa NPs containing DiO (0.15 mg mL^{-1}) were diluted to 1 mL with pure fresh water. Experiments in a spectrofluorimeter Varian Cary Eclipse (Palo Alto, CA, USA) were carried out by excitation of the donor at 470 nm and measuring the emission from 480 to 650 nm with constant magnetic stirring at 37 °C for 24 h.

GSH experiment. The same experiment was repeated adding the necessary mg of GSH to the cell to be at 10 mM after 3 h of experiment.

PC–Chol liposomes experiment. The same experiment was repeated adding 10 μL of 100 mg mL^{-1} PUUa NPs containing DiI (0.15 mg mL^{-1}) and 10 μL of 100 mg mL^{-1} PUUa NPs containing DiO (0.15 mg mL^{-1}) to 1 mL 10 mM solution of PC–Chol liposomes 0.45 μm syringe-filtered.

2.4.9. MALDI-TOF MS. B3100–cRGDfK conjugate formation was followed using MALDI-TOF MS. The experiment was carried out on an Applied Biosystems Voyager-DETMRP mass spectrometer (Waltham, MA, USA), using α-cyano-4-hydroxycinnamic acid (ACH) as a matrix. B3100 and B3100–cRGDfK at 1 mg mL^{-1} after 2 h of reacting were analysed.

2.4.10. NMR. NMR spectra were recorded on a Varian Mercury (400 MHz) (Agilent) (Santa Clara, CA, USA). Reactive prepolymers Hyfil, Amphil and Hyfob were previously dissolved in $CDCl_3$ at 100 mg mL^{-1}.

2.4.11. Lyophilization and redispersion procedures. Previously dialysed samples (100 mg mL^{-1}) were lyophilized and directly redispersed at the desired concentration by overnight stirring at 1500 rpm. Lyophilized and redispersed samples were examined by TEM and DLS to ratify optimal size and morphology characteristics.

2.5. Biological studies

2.5.1. Integrin expression characterization. The expression of $\alpha_v\beta_3$ and $\alpha_v\beta_5$ was analyzed by flow cytometry using monoclonal antibodies against both heterodimers (MAB1976H and MAB1961F from Millipore). Specifically, the cell suspensions detached using PBS–EDTA (5 mM) were incubated with 3 μg of $\alpha_v\beta_3$ antibody. 1 μg of $\alpha_v\beta_5$ antibody for 20 min at 4 °C, and IgG2 isotype controls from eBioscience (San Diego, CA, USA) were included. Cells were analyzed using FacScalibur Becton Dickinson (Franklin Lakes, NJ, USA) and FCS Express 4 software De Novo Software (Los Angeles, CA, USA).

2.5.2. Cell internalization by flow cytometry. The time dependent internalization of targeted and non-targeted PUUa NPs was studied using flow cytometry. Specifically, exponentially grown cultures were detached using PBS–EDTA (5 mM), resuspended in Ca^{2+} and Mg^{2+} free PBS and incubated at 37 °C with a final concentration of 38.5 μg mL^{-1} of NPs containing 10 μg mL^{-1} of Dil. After incubation, cells were washed twice with PBS and stained with DAPI (50 μg mL^{-1}) to include only viable cells in the analysis. Cells were analyzed using LRS Fortessa Becton Dickinson (Franklin Lakes, NJ, USA) and FCS Express 4 software De Novo Software (Los Angeles, CA, USA).

2.5.3. Cell internalization and lysosomal colocalization by confocal microscopy. Cells were seeded in 24 well-plates containing coverslips (50 000 cells per well) and left overnight at 37 °C with 5% CO_2 to allow cell attachment. Cells were then washed carefully with PBS and 1 μg mL^{-1} of Dil containing PUUa NPs (with or without RGD targeting moieties) were added to the cultures diluted in complete cell growing media. After the incubation period, cells were washed twice with PBS and stained for 15 min with 10 μM LysoTracker Green (Life Technologies) and directly visualized using a confocal microscope (FV1000, Olympus). Confocal images of the same *Z* plane were obtained for LysoTracker (green signal) and for DiI (red signal), using excitation peaks at 488/561 nm and emission at 522/585 nm for LysoTracker and Dil, respectively and merged afterwards to demonstrate that some of the nanoparticles are located inside acidic organelles labeled by LysoTracker. Images were acquired at 60× magnification. Quantification of the NP signal outside the lysosomes was performed using Fiji ImageJ[22] (NIH, Bethesda, MD, USA) with confocal images taken from at least three different fields. The red signal in every cell in each field (8–14) was quantified for each *Z*-plane, and then compared statistically using the *t*-Student test with GraphPad software (La Jolla, CA, USA).

Cytotoxicity studies. The *in vitro* cytotoxicity of the NPs was tested by the 3-[4,5-dimethylthiazol-2-yl]-2,5-diphenyltetrazolium bromide (MTT) method after 72 h incubation.[23]

3. Results and discussion

As we have shown in our recent methodological patent many nanoparticles with multiple structural and biological functionalities can be obtained due to the versatile polyurethane chemistry. In fact, the novel kind of NPs based on reactive polyurethane and polyurea prepolymers introduced herein allowed controlled stratification at the nano-interface and tunable functionality in their multiwalled structure[24] (Fig. 1a and b). As proof of concept for cancer therapy, disulfide bonds were successfully included in the prepolymers to enable tailored degradation and controlled intracellular release of encapsulated hydrophobic

 This journal is © The Royal Society of Chemistry 2015

Published on 24 August 2015. Downloaded by Universitat de Barcelona on 04/09/2015 11:30:50.

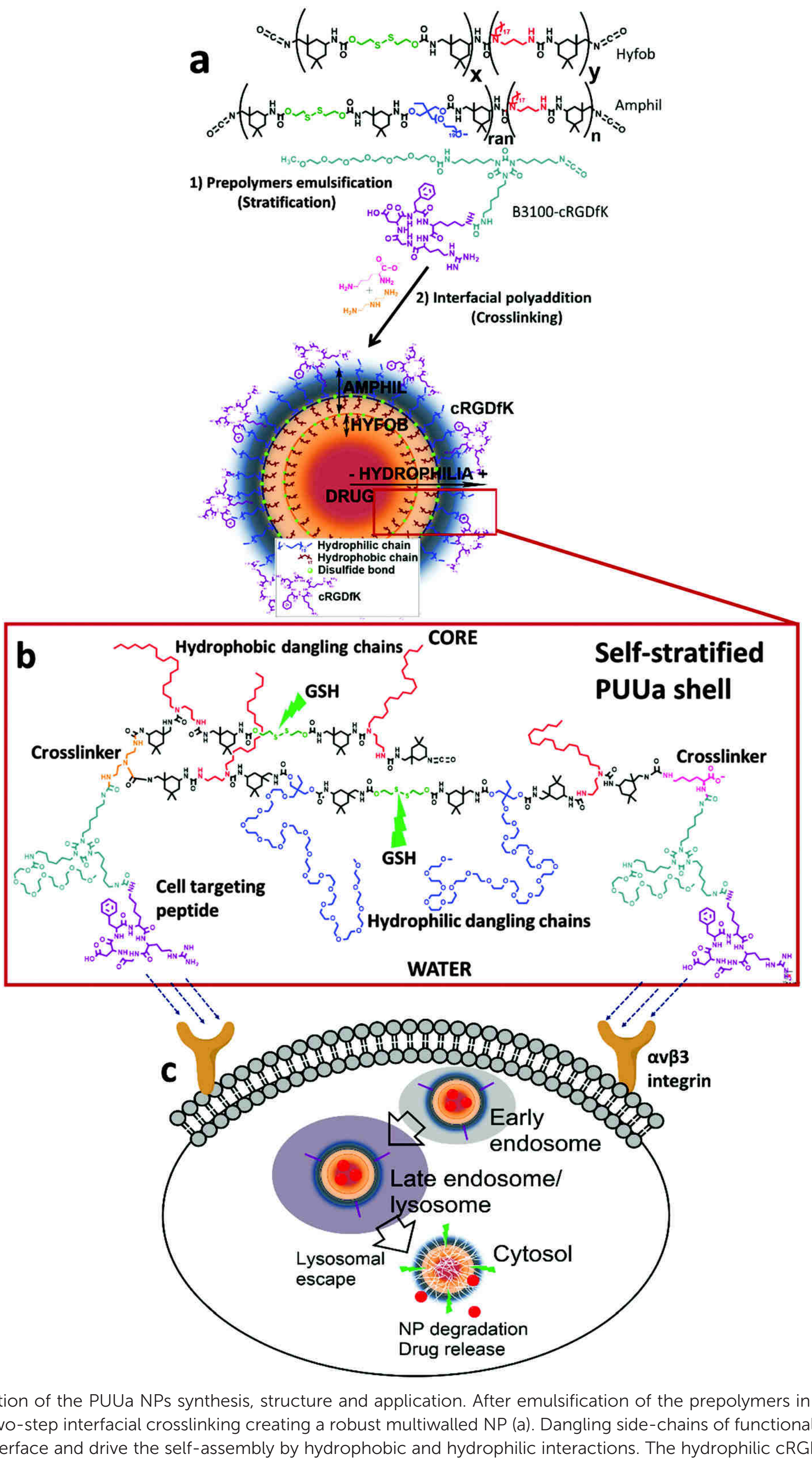

Fig. 1 Schematic illustration of the PUUa NPs synthesis, structure and application. After emulsification of the prepolymers in water, the self-stratified shell is consolidated by two-step interfacial crosslinking creating a robust multiwalled NP (a). Dangling side-chains of functional prepolymers self-orient through the oil–water interface and drive the self-assembly by hydrophobic and hydrophilic interactions. The hydrophilic cRGDfK peptide is covalently linked *via* urea bonds to the more external part of the shell (b). Scheme of the PUUa NP receptor mediated internalization and cytosolic delivery of hydrophobic cargo (c).

Published on 24 August 2015. Downloaded by Universitat de Barcelona on 04/09/2015 11:30:50.

molecules at intracellular GSH concentration. Moreover, a cyclic hydrophilic RGD peptide located on the outer shell of the NP was selected and innovatively conjugated to mediate specific targeting to cells overexpressing $\alpha_v\beta_3$ integrin (Fig. 1c). Finally, to strengthen this stratified structure a crosslinking step with polyamines was key to form an isocyanate-free, ordered and robust nanostructure.[25–27]

Thus, we synthesized two new reactive prepolymers by successive quantitative polyaddition reactions of difunctional monomers with an aliphatic diisocyanate (isophorone diisocyanate) (see monomers description in the ESI† and Fig. S1 and Table S1) and characterized them using automatic titration (Fig. S2, ESI†), FT-IR (Fig. S3 and S4, ESI†) and NMR (Fig. S5 and S6 in the ESI†). On one hand, the reactive amphiphilic prepolymer (Amphil) contained disulfide bonds (2-hydroxyethyl disulfide) in the main chain, hydrophilic (polyethylene glycol monomethyl ether) and hydrophobic (*N*-Coco-1,3-propylenediamine) dangling side-chains and terminal isocyanate groups. The hydrophilic side-chains self-oriented toward the aqueous surrounding media and emulsified in water the whole pre-formed PUUa NP. The hydrophobic chains stabilized and encapsulated the inner hydrophobic prepolymer (Hyfob, see below) and the oily core by hydrophobic interactions. Thus, Amphil worked as an all-in-one polymer ensuring oil and water miscibility, redox-degradability and isocyanate reactivity. On the other hand, the hydrophobic reactive prepolymer (Hyfob) bore disulfide bonds in the main chain, terminal isocyanate groups and just the hydrophobic dangling side-chains. The idea to introduce Hyfob in the shell was based on the wish to prevent premature leakage of the encapsulate without renouncing the redox-degradability. In this regard, to achieve this hydrophobically stratified structure, it was also crucial to use a 5% (w/w) of an ultrahydrophobe as a core material, such as the biocompatible capric–caprylic triglyceride (Crodamol GTCC). Its solubilizing effect on hydrophobic therapeutically active molecules[28] and ability to decrease coacervation of oily core nanoparticles due to the Ostwald ripening effect[29] made it the product of choice. In addition, as introduced previously, to convert these hydrophobically driven self-stratified structures into covalently stable isocyanate-free PUUa NPs, the reactive polymeric shell was crosslinked with small polyamines (Fig. S7 in the ESI†). Hence, as seen from Fig. 2 we observed that addition of L-lysine (Lys), a diaminocarboxylate moiety, into the emulsified reactive prepolymers as a pre-crosslinker and extender, reduced the NP size as a result of the enhanced internal emulsifying effect of carboxylate[30,31] compared to NPs carrying only polyethylene glycol monomethyl ether (YMER N-120) as a hydrophilic precursor. Finally, in any of the formulations the shell was consolidated by a highly reactive small triamine, diethylenetriamine (DETA) (Fig. S8 in the ESI† prove isocyanates disappearance using FT-IR after the crosslinking reaction). At this point, with the aim of investigating our system cell targeting specificity, a novel method was developed to anchor the broadly used hydrophilic cRGDfK cyclic pentapeptide to our PUUa NPs *via* urea linkage without loss of bioactivity.[32] The Bayhydur 3100 hydrophilic polyisocyanate linker[33] (B3100) and cRGDfK free primary amino group of the Lys residue were effectively coupled in aqueous media (pH 10, 5 °C) (Fig. S9 in the ESI†). By optimizing the reaction stoichiometry we were able to maintain free NCO moieties in the conjugate for further PUUa NP functionalization with only one peptide per linker molecule, as

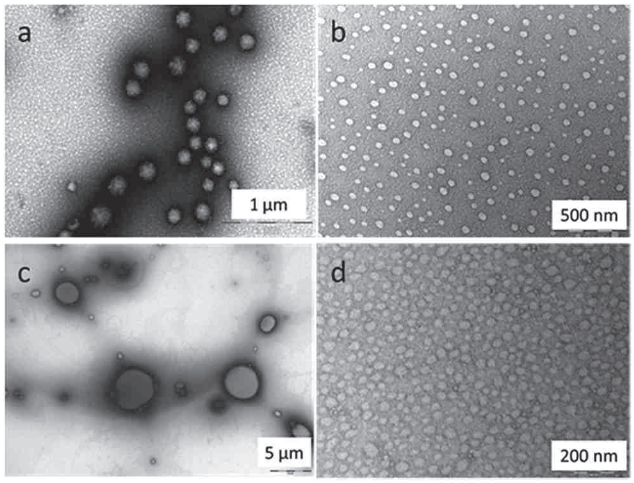

Multiwalled Samples	Diameter (nm)	SD (nm)	PDI
a) DETA-crosslinked PUUa NP	170.3	32.0	0.04
b) Lys-crosslinked PUUa NP	53.2	22.8	0.18
c) Non-crosslinked PUUa NP	207.7	590.8	5.91
d) Lys-DETA-crosslinked PUUa NP	29.0	5.0	0.03

Fig. 2 TEM micrographs of multiwalled PUUa NPs showing the importance of the crosslinking process to get a monodisperse sample. After emulsification of the reactive prepolymers in water, PUUa NPs were crosslinked by successive additions of Lys and/or DETA, respectively (a, b and d). Non-crosslinked PUUa NPs were kept under magnetic stirring for 3 days until the isocyanate group disappeared from the IR spectra due to the reaction with water. It can be observed that without a crosslinker, NPs are not interfacially stabilized and a highly polydisperse sample is obtained (c). Images were statistically analyzed by random recording of 5 different zones of the copper grid.

followed using MALDI-TOF MS experiments (Fig. S10 in the ESI†). Furthermore, PUUa NP functionalization with the B3100–cRGDfK conjugate (PUUa NP–RGD) occurred in high yield (98.5%), as quantified by the HPLC calibration curve (Table S2 in the ESI†). Then, the B3100–cRGDfK isocyanate reactive conjugate was fixed in the prepolymeric shell *via* the previously explained crosslinking step yielding around 2% cRGDfK per PUUa NP. Transmission Electron Microscopy (TEM) and Dynamic Light Scattering (DLS) revealed monomodal size distributions of about 20 nm for PUUa NP-DiI and PUUa NP-DiI–RGD (Fig. 3a and b). Zeta potential (Zpot) measurements of dialysis-purified nanoparticles exhibited similar slightly negative surface charges due to Lys carboxylate outer shell localization (Fig. 3e). This experimental result further corroborated the shell self-stratified nanostructure by hydrophobic interactions. In addition, the multiwalled nanoparticles robust structure and hydrophilic surface made them lyophilizable and redispersable in aqueous media without cryoprotectants.‡

‡ All data presented belongs to experiments performed with lyophilized and redispersed multiwalled PUUa NPs (for more details see Section 3 in ESI†).

 This journal is © The Royal Society of Chemistry 2015

Published on 24 August 2015. Downloaded by Universitat de Barcelona on 04/09/2015 11:30:50.

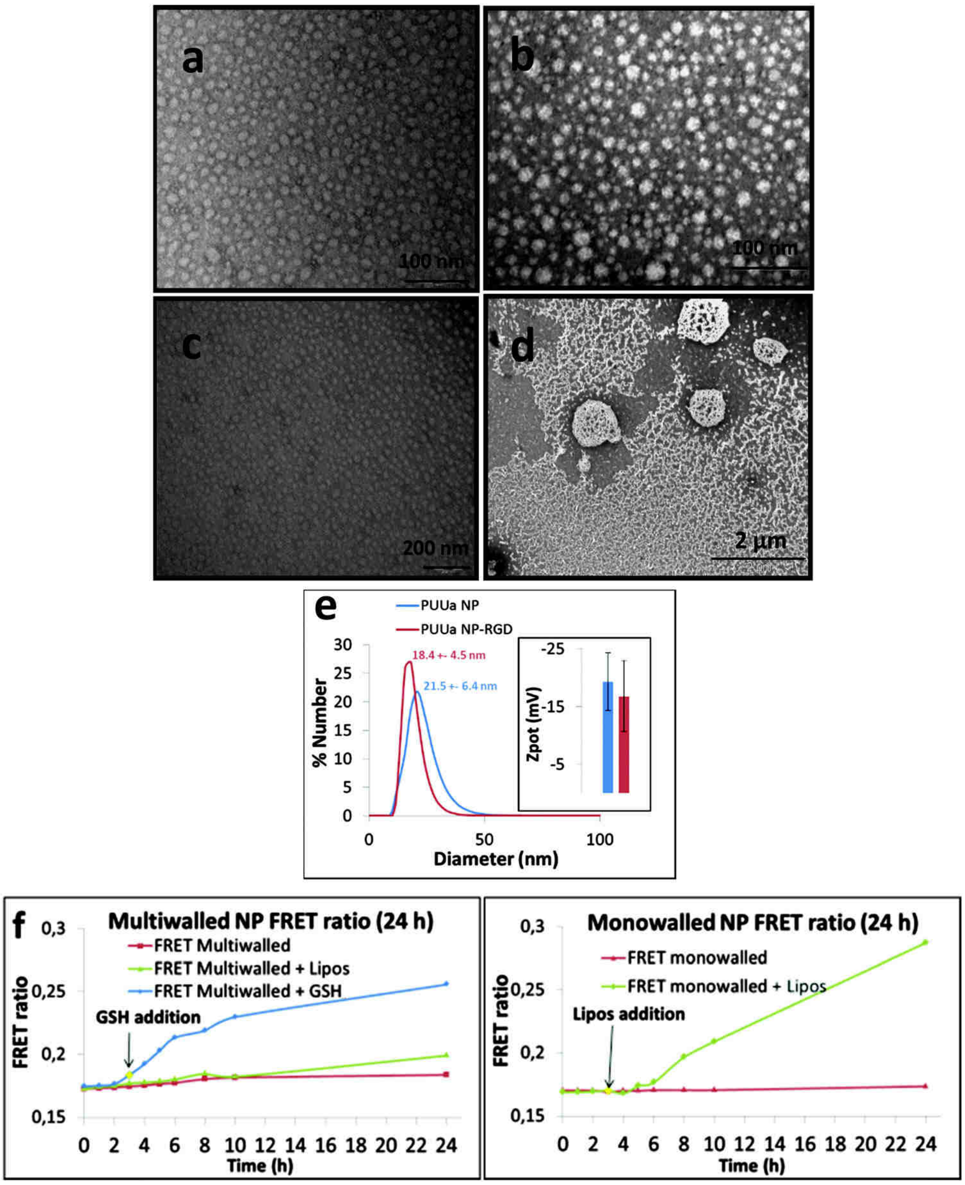

Fig. 3 TEM images of multiwalled PUUa NPs (a) and PUUa NP–RGD (b). TEM images of PUUa NPs before (c) and after treatment with GSH 10 mM at 37 °C for 24 h (d). After treatment with GSH the clear degradation of the PUUa NPs is achieved and degraded polymers form aggregates up to 1 μm in size. (e) Hydrodynamic diameter measured by DLS and the zeta potential of PUUa NP–RGD (blue) and PUUa NPs (red). Release dynamics comparison between multiwalled and monowalled PUUa NPs (f). Aqueous media (red), *in vivo*-like media (green) and 10 mM reduced GSH (blue).

Shell biodegradability and specific cargo release are fundamental features in drug delivery systems. To this end, the presence of disulfide bonds in the shell can facilitate polymer degradation by reductive enzymes and peptides overexpressed in the cytosolic environment of tumor cells.[34] Concretely, glutahione tripeptide has an intracellular concentration of 2–10 mM in the cytosol while the extracellular concentration is about 2–20 μM. Taking advantage of this intracellular concentration, the PUUa NP degradation and cargo release under reductive conditions were studied by transmission electron microscopy (TEM) and Förster resonance energy transfer (FRET) techniques, respectively. Thus, the NP degradation was determined using TEM before and after a 24 h treatment with 10 mM GSH. Significant differences in size were detected due to polymer aggregate formation after redox-triggered degradation (Fig. 3c and d). To confirm the differences of the release properties of multiwalled and monowalled nanostructures, first, the monowalled NPs were morphologically characterized by TEM (Fig. S11, ESI†) and then, FRET experiments where performed in different media. Thus, we encapsulated two typical cell membrane staining agents[35] as fluorescent lipophilic cargo, namely DiI and DiO, in separate PUUa NPs. As already described by the FRET mechanism, changes in the fluorophore proximity allowed us to evaluate the release dynamics and potential leakiness of different PUUa NPs.[36] So, both fluorescent probes were encapsulated at a total concentration of 0.15% w/w

Published on 24 August 2015. Downloaded by Universitat de Barcelona on 04/09/2015 11:30:50.

to avoid static quenching[37] (encapsulation efficiency 100%, data not shown). PUUa NP-DiI and PUUa NP-DiO were then mixed (FRET PUUa NPs) and the FRET ratio was represented against time as $I_a/(I_d + I_a)$, where I_a was the maximum intensity of the acceptor and I_d the maximum intensity of the donor. The slope of the linear fit was defined as the release coefficient at 37 °C for the first 10 h of the experiment (Fig. S13 in the ESI†). For both multiwalled and monowalled NPs the release coefficient appeared to be almost negligible in water (0.001 h^{-1} and 0.0001 h^{-1} respectively), which corroborated their outstanding encapsulation stability. Further, as the PUUa NPs are expected to stably encapsulate the lipophilic drug until reaching the cytosol of the tumor cell, we wanted to check that the cargo would not be released unspecifically during cell internalization. With this in mind, we sought to mimic a cellular microenvironment by mixing egg phosphatidylcholine–cholesterol previously reported liposomes (Lipos)[38] (2 : 1 w/w) with our FRET PUUa NPs (10 mM). Confirming our expectations, multiwalled NPs were stable during the first 10 h (0.001 h^{-1}), but monowalled NPs exhibited a pronounced increase of the FRET ratio upon mixing with Lipos (0.007 h^{-1}) due to unspecific release. Additionally, under treatment with 10 mM GSH, multiwalled PUUa NPs clearly showed a FRET increase (0.01 h^{-1}) caused by disulfide bond cleavage and the sudden release and mixing of the fluorophores (see Fig. 3f and Fig. S12 in the ESI†). In a final proof of principle study, we first tested that the PUUa NPs were not cytotoxic to cells (Fig. S14 in the ESI†) and then internalization assays were performed. To that end, the PUUa NPs were incubated with HT-29 and U87-MG cancer cells, known to have very low and high expression of $\alpha_v\beta_3$ integrins, respectively (Table S2, ESI†). Flow cytometry and confocal studies revealed that, due to the RGD outer localization in the multiwalled structure, the PUUa NP–RGD encapsulating DiI fluorophore (PUUa NP-DiI–RGD) entered $\alpha_v\beta_3$ integrin expressing cells more efficiently (Fig. 4a) than non-functionalized ones. Moreover, the internalization of PUUa NP-DiI–RGD in $\alpha_v\beta_3$-negative HT-29 cells was similar to non-targeted NPs, indicating that the enhanced uptake of cRGDfK functionalized NPs observed in U87-MG cells was specific.

Confocal images also showed colocalization of the NPs with lysosomal markers (LysoTracker Green), confirming that the NPs entered cells through the endocytic pathway, and that the uptake and the lysosomal colocalization was clearly enhanced

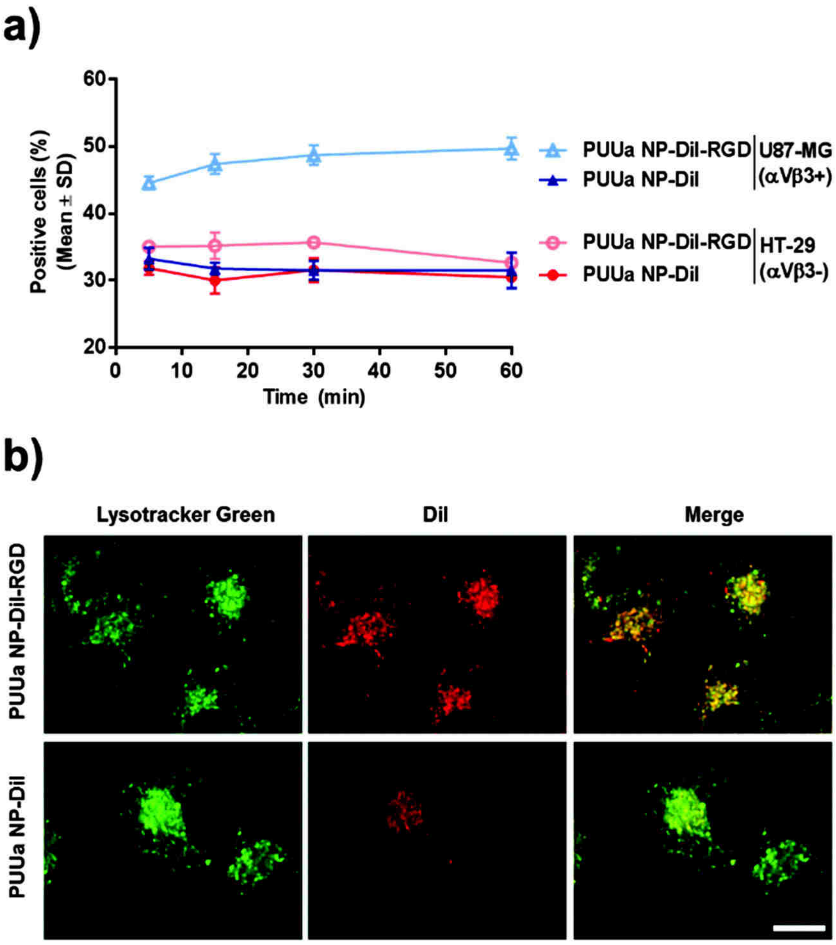

Fig. 4 PUUa NP internalization. (a) Flow cytometry studies were performed in U87-MG ($\alpha_v\beta_3$-positive) and HT-29 ($\alpha_v\beta_3$-negative) cancer cells at different time points with 10 μg of mL^{-1} DiI (38.5 μg mL^{-1} of NPs). (b) Confocal images of U87-MG cells incubated for 24 h with 1 μg mL^{-1} of DiI and stained with LysoTracker Green to show the lysosomal localization of the PUUa NPs. Magnification bar corresponds to 10 μm.

This journal is © The Royal Society of Chemistry 2015

Published on 24 August 2015. Downloaded by Universitat de Barcelona on 04/09/2015 11:30:50.

in the case of PUUa NP-DiI–RGD (Fig. 4b). In order to trace the final cytosolic release of the NPs cargo, U87-MG cells were incubated for 1 h with PUUa NP-DiI–RGD, washed thoroughly and observed immediately and 24 h later. The initially observed distinctive punctuated signal corresponding to the lysosomal localization changed to a more diffuse uniform fluorescent cell cytoplasm distribution, which, in line with the above mentioned FRET experiments proved that our system was able to escape from the lysosome and spread their cargo through the cytosol (Fig. S15 in the ESI†).

In conclusion, we have depicted a novel methodology to develop self-stratified PUUa NPs based on the amphiphilic properties of differently designed prepolymers, and we have clearly evidenced the better encapsulation ability of multi-walled NPs compared to their monowalled counterparts. This multiwalled structure has been experimentally proved by FRET studies, Zeta potential measurements and cell internalization experiments. The use of L-lysine as an extender or pre-crosslinker modulated the size of the micelles reaching very small entities that finally were stabilized by crosslinking with DETA. Cargo delivery and nanoparticle shell degradability were also controlled by incorporating DEDS, a redox moiety that responded to intracellular glutathione. The use of a specifically designed reactive conjugate containing a hydrophilic RGD peptide ensured the straightforward functionalization of the outer part of the nanoparticle shell. These systems convey a multiwalled nanostructure with on-demand release properties and cancer cell targeting behavior. This confirms that our PUUa NPs are outstanding platforms for smart drug delivery and opens up a new era in nanostructured systems with multiple targeting and degradation possibilities that generate an enormous range of application opportunities. New characterization techniques are being explored to visually prove the sub-30 nm self-stratified structures. Biological studies with a variety of antitumor drugs are also underway.

Acknowledgements

We gratefully acknowledge MICINN and FEDER (IPT-090000-2010-0001), CICYT (CTQ2012-30930) and the Generalitat de Catalunya (2009SGR 1024).

Notes and references

1 V. P. Torchilin, *Nat. Rev. Drug Discovery*, 2014, **13**, 813–827.
2 N. Kamaly, Z. Xiao, P. M. Valencia, A. F. Radovic-Moreno and O. C. Farokhzad, *Chem. Soc. Rev.*, 2012, **41**, 2971–3010.
3 K. Landfester, *Angew. Chem., Int. Ed.*, 2009, **48**, 4488–4507.
4 F. Tiarks, K. Landfester and M. Antonietti, *Langmuir*, 2001, **17**, 908–918.
5 L. Wu and J. Baghdachi, *Functional Polymer Coatings: Principles, Methods, and Applications*, WILEY-VCH Verlag GmbH, 2015.
6 Z. Zhang, R. L. Marson, Z. Ge, S. C. Glotzer and P. X. Ma, *Adv. Mater.*, 2015, **27**, 3947–3952.
7 D. K. Chattopadhyay and K. V. S. N. Raju, *Prog. Polym. Sci.*, 2007, **32**, 352–418.
8 J. Y. Cherng, T. Y. Hou, M. F. Shih, H. Talsma and W. E. Hennink, *Int. J. Pharm.*, 2013, **450**, 145–162.
9 B. K. Kim and J. C. Lee, *Polymer*, 1996, **37**, 469–475.
10 S.-H. Son, H.-J. Lee and J.-H. Kim, *Colloids Surf., A*, 1998, **133**, 295–301.
11 A. M. Heming, P. J. Mulqueen, H. B. Scher and I. M. Shirley, *Use of Reactive Polymeric Surfactants in the Formation of Emulsions*, US7199185 B2, 2002, PCT/GB2002/002744, 2002.
12 J. Andrieu, N. Kotman, M. Maier, V. Mailänder, W. S. L. Strauss, C. K. Weiss and K. Landfester, *Macromol. Rapid Commun.*, 2012, **33**, 248–253.
13 M. Ding, N. Song, X. He, J. Li, L. Zhou, H. Tan, Q. Fu and Q. Gu, *ACS Nano*, 2013, **7**, 1918–1928.
14 U. Paiphansiri, J. Dausend, A. Musyanovych, V. Mailänder and K. Landfester, *Macromol. Biosci.*, 2009, **9**, 575–584.
15 S. A. Guelcher, *Tissue Eng., Part B*, 2008, **14**, 3–17.
16 L. T. Budnik, D. Nowak, R. Merget, C. Lemiere and X. Baur, *J. Occup. Med. Toxicol.*, 2011, **6**, 9.
17 S. A. Guelcher, K. M. Gallagher, J. E. Didier, D. B. Klinedinst, J. S. Doctor, A. S. Goldstein, G. L. Wilkes, E. J. Beckman and J. O. Hollinger, *Acta Biomater.*, 2005, **1**, 471–484.
18 P. Zou, H. Chen, H. J. Paholak and D. Sun, *Mol. Pharmaceutics*, 2013, **10**, 4185–4194.
19 X. Dai, Z. Su and J. O. Liu, *Tetrahedron Lett.*, 2000, **41**, 6295–6298.
20 I. R. Clemitson, *Castable Polyurethane Elastomers*, CRC Press, 2008.
21 A. Prabhakar, D. K. Chattopadhyay, B. Jagadeesh and K. V. S. N. Raju, *J. Polym. Sci., Part A: Polym. Chem.*, 2005, **43**, 1196–1209.
22 J. Schindelin, I. Arganda-Carreras, E. Frise, V. Kaynig, M. Longair, T. Pietzsch, S. Preibisch, C. Rueden, S. Saalfeld, B. Schmid, J.-Y. Tinevez, D. J. White, V. Hartenstein, K. Eliceiri, P. Tomancak and A. Cardona, *Nat. Methods*, 2012, **9**, 676–682.
23 P. Botella, I. Abasolo, Y. Fernández, C. Muniesa, S. Miranda, M. Quesada, J. Ruiz, S. Schwartz and A. Corma, *J. Controlled Release*, 2011, **156**, 246–257.
24 J. Rocas Sorolla and P. Rocas Alonso, *Process for the Manufacture of a Microencapsulated and Reactive Amphiphilic Compound, and Corresponding Microencapsulated Composition*, WO2014114838 A3, 2014.
25 X. Yan, M. Delgado, A. Fu, P. Alcouffe, S. G. Gouin, E. Fleury, J. L. Katz, F. Ganachaud and J. Bernard, *Angew. Chem., Int. Ed.*, 2014, 1–5.
26 J.-W. Yoo, N. Doshi and S. Mitragotri, *Adv. Drug Delivery Rev.*, 2011, **63**, 1247–1256.
27 K. Landfester and V. Mailänder, *Expert Opin. Drug Delivery*, 2013, **10**, 593–609.
28 R. G. Strickley, *Pharm. Res.*, 2004, **21**, 201–230.
29 K. Landfester, N. Bechthold, F. Tiarks and M. Antonietti, *Macromolecules*, 1999, **32**, 5222–5228.
30 P. Ni, M. Zhang and N. Yan, *J. Membr. Sci.*, 1995, **103**, 51–55.
31 G. Morral-Ruíz, C. Solans, M. L. García and M. J. García-Celma, *Langmuir*, 2012, **28**, 6256–6264.

Published on 24 August 2015. Downloaded by Universitat de Barcelona on 04/09/2015 11:30:50.

32 R. Haubner, R. Gratias, B. Diefenbach, S. L. Goodman, A. Jonczyk and H. Kessler, *J. Am. Chem. Soc.*, 1996, **118**, 7461–7472.
33 A. M. Heming, P. J. Mulqueen, H. B. Scher and I. M. Shirley, *Use of Reactive Polymeric Surfactants in the Formation of Emulsions*, US7199185 B2, 2002.
34 R. Cheng, F. Feng, F. Meng, C. Deng, J. Feijen and Z. Zhong, *J. Controlled Release*, 2011, **152**, 2–12.
35 R. W. Sabnis, *Handbook of Biological Dyes and Stains: Synthesis and Industrial Applications*, 2010.
36 S. Jiwpanich, J.-H. Ryu, S. Bickerton and S. Thayumanavan, *J. Am. Chem. Soc.*, 2010, **132**, 10683–10685.
37 H. Chen, S. Kim, L. Li, S. Wang, K. Park and J.-X. Cheng, *Proc. Natl. Acad. Sci. U. S. A.*, 2008, **105**, 6596–6601.
38 T. M. Allen and A. Chonn, *FEBS Lett.*, 1987, **223**, 42–46.

This journal is © The Royal Society of Chemistry 2015